Published in final edited form as:
*Science*. ; 369(6504): . doi:10.1126/science.aaz2532.

# The proteasome controls ESCRT-III-mediated cell division in an archaeon

**Gabriel Tarrason Risa**[#1], **Fredrik Hurtig**[#2], **Sian Bray**[3], **Anne E. Hafner**[1,4,5], **Lena Harker-Kirschneck**[1,4,5], **Peter Faull**[6], **Colin Davis**[6], **Dimitra Papatziamou**[7], **Delyan R. Mutavchiev**[1], **Catherine Fan**[1], **Leticia Meneguello**[1], **Andre Arashiro Pulschen**[1], **Gautam Dey**[1], **Siân Culley**[1], **Mairi Kilkenny**[3], **Diorge P. Souza**[1], **Luca Pellegrini**[3], **Robertus A. M. de Bruin**[1], **Ricardo Henriques**[1], **Ambrosius P. Snijders**[6], **Anđela Šarić**[1,4,5], **Ann-Christin Lindås**[2], **Nicholas P. Robinson**[7,†], **Buzz Baum**[1,4,†]

[1]MRC-Laboratory for Molecular Cell Biology, University College London (UCL), London, UK

[2]Department of Molecular Biosciences, The Wenner-Gren Institute, Stockholm University, Stockholm, Sweden

[3]Biochemistry Department, University of Cambridge, Cambridge, UK

[4]Institute for the Physics of Living Systems, UCL, London, UK

[5]Department of Physics and Astronomy, UCL, London, UK

[6]Proteomics Platform, The Francis Crick Institute, London, UK

[7]Faculty of Health and Medicine, Division of Biomedical and Life Sciences, Lancaster University, Lancaster, UK

[#] These authors contributed equally to this work.

## Abstract

*Sulfolobus acidocaldarius* is the closest experimentally tractable archaeal relative of eukaryotes and, despite lacking obvious cyclin-dependent kinase and cyclin homologs, has an ordered eukaryote-like cell cycle with distinct phases of DNA replication and division. Here, in exploring the mechanism of cell division in *S. acidocaldarius*, we identify a role for the archaeal proteasome in regulating the transition from the end of one cell cycle to the beginning of the next. Further, we identify the archaeal ESCRT-III homolog, CdvB, as a key target of the proteasome and show that its degradation triggers division by allowing constriction of the CdvB1:CdvB2 ESCRT-III division

[†]**Corresponding author**: b.baum@ucl.ac.uk (B.B.); n.robinson2@lancaster.ac.uk (N.P.R.).

**Author contributions:** B.B. and G.T.R. conceived the study. Initial observations were made by F.H. and G.T.R. Structural work was planned and carried out by S.B. and N.P.R., with assistance from M.K. and L.P. In vitro proteasome assays were planned and performed by D.P. and N.P.R. Cell biology methods and experiments were developed by G.T.R., F.H., G.D., D.R.M., and S.C. with guidance from B.B., R.H., and A.-C.L. Molecular genetics were done by F.H., D.R.M., A.A.P., and G.T.R. Biochemical analysis was carried out by F.H., G.T.R., L.M., A.A.P., and D.P.S. RNA analysis was carried out by C.F., with guidance from B.B. and R.A.M.d.B. Mass spectrometry preparation and analysis was carried out by P.F., C.D., and G.T.R., with guidance from A.P.S. The physical model was built by A.E.H. and L.H.-K., with guidance from A.Š. and B.B. The paper was written by G.T.R., F.H., and B.B., with input from all other authors.

**Competing interests:** The authors declare no competing interests.


Europe PMC Funders Author Manuscripts

ring. These findings offer a minimal mechanism for ESCRT-III-mediated membrane remodeling and point to a conserved role for the proteasome in eukaryotic and archaeal cell cycle control.





The eukaryotic cell cycle is ordered by oscillations in the activity of a conserved set of cyclin-dependent kinases. Although both cyclins and cyclin-dependent kinases have yet to be identified outside of eukaryotes, *Sulfolobus acidocaldarius*, a member of the TACK (Thaumarchaeota, Aigarchaeota, Crenarchaeota, and Korarchaeota) superphylum of Archaea, possesses an ordered cell cycle with distinct phases of DNA replication and division, similar in structure to the cell cycle observed in many eukaryotes (1). Several of the enzymes used to drive key events in the cell cycle are also conserved from archaea to eukaryotes. For example, archaeal homologs of eukaryotic Cdc6, Orc, MCM, and GINS proteins initiate DNA replication at multiple origins in *S. acidocaldarius*, just as they do in eukaryotes (2, 3). Additionally, previous work shows that homologs of ESCRT-III and the AAA+ adenosine triphosphatase (ATPase) Vps4, proteins that mediate abscission and other membrane remodeling processes in eukaryotes, play an important role in TACK archaeal cell division (4). These observations beg the question: Are any of these common events regulated by conserved elements of the cell cycle control machinery that are shared across archaea and eukaryotes?

Although archaea lack clear homologs of both cyclins and cyclin-dependent kinases, archaeal homologs of the 20S core eukaryotic proteasome are readily identifiable (5–8). In eukaryotes, cell division is initiated by activation of the ubiquitin-E3 ligase, APC, which triggers proteasome-mediated degradation of cyclin B and securin and likely a host of other proteins (9), leading to irreversible mitotic exit (10), chromosome segregation, and cytokinesis (11,12). This led us to test whether proteasome-mediated degradation also plays a role in regulating the cell cycle reset in TACK archaea (1).

Here, we report that proteasomal activity is required for *S. acidocaldarius* cell division, using inhibitors of the 20S proteasome. Proteomics analyses identified a single archaeal ESCRT-III homolog, CdvB (Saci_1373), as a key target for proteasome-mediated degradation during the final stages of the cell division cycle. CdvB is part of the CdvABC operon (Saci_1374, Saci_1373, and Saci_1372) and has previously been implicated in *S. acidocaldarius* cell division (13–15). A combination of microscopy and flow cytometry data further suggest that CdvB both templates the assembly of a contractile ESCRT-III copolymer, composed of the paralogs CdvB1 (Saci_0451) and CdvB2 (Saci_1416), and prevents their constriction. As a consequence, proteasome-mediated degradation of CdvB triggers cell division.

## Results

### Bortezomib inhibits the *S. acidocaldarius* proteasome

To determine a detailed structure of the *S. acidocaldarius* proteasome, building on previous work (16), we coexpressed the α subunit and N-terminally truncated β subunit of the proteasome (Saci_0613 and Saci_0662ΔN). This enabled us to produce diffracting crystals of the catalytically inactive, 28-subunit 20S proteasome, allowing us to determine its structure to a resolution of 3.7 Å [Fig. 1A; figs. S1, A to C, and S2, A to C; and table S1;

Protein Data Bank (PDB) ID 6Z46]. Structures of the equivalent complexes from the euryarchaeon *Archaeoglobus fulgidus* (PDB ID 1J2Q) and *Saccharomyces cerevisiae* (PDB ID 4NNN) were then used to generate a homology model of an N-terminally truncated catalytically active β subunit (Saci_0909ΔN), which was docked into the structure of the *S. acidocaldarius* proteasome in place of one inactive β subunit (Saci_0662 ΔN) (see methods) (17). It was then possible to dock bortezomib (PS-341, Velcade), an established small-molecule inhibitor of the proteasomes of euryarchaeota and eukaryotes (18–20), into the model's active site (Fig. 1B and fig. S1, D and E). Here, the boronic acid moiety of bortezomib forms a bond with the nucleophilic hydroxyl group of the active site threonine, indicating that the small molecule is likely able to inhibit the proteolytic activity of the *S. acidocaldarius* 20S proteasome as it does in eukaryotes and in the euryarchaeon *Haloferax volcanii* (20,21).

To determine whether bortezomib can inhibit the *S. acidocaldarius* proteasome in vitro, as suggested by this structural analysis, we examined the ability of the active complex [consisting of α subunits, together with N-terminally truncated structural and catalytically active β subunits(Saci_0613/Saci_0662ΔN/Saci_0909ΔN)] to degrade a Urml-tagged green fluorescent protein (GFP) substrate, using a biochemical setup we described previously (see methods) (16). When this assay was carried out with different concentrations of inhibitor, the rate of substrate degradation was diminished (Fig. 1C and fig. S3, A to D). We then mutated a conserved valine residue (V49) that mediates critical contacts between the active site and the inhibitor (22) to a threonine (V49T). As expected, this led to a reduction in the sensitivity of the purified *S. acidocaldarius* 20S proteasome to bortezomib (fig. S3, E and F), validating the mode of inhibitor action.

## Proteasomal inhibition arrests the cell cycle of S. acidocaldarius

Having demonstrated that bortezomib inhibits the *S. acidocaldarius 20S* proteasome activity in vitro, bortezomib was added to *S. acidocaldarius* cultures to look for a possible role for the 20S proteasome in cell cycle control. For this experiment, cells were synchronized to $G_2$ using acetic acid, released, and observed by flow cytometry as they reentered the cell cycle and divided (see methods) (23). Notably, when bortezomib was added to cultures 80 min after release from the acetic acid arrest, the cells failed to divide (Fig. 1D and fig. S4, A and B). Furthermore, this bortezomib-induced cell cycle arrest was accompanied by a twofold enrichment in the number of cells harboring compact and separated nucleoids [relative to those treated with the dimethyl sulfoxide (DMSO) solvent; Fig. 1, E and F]. Although a similar arrest was observed in cells treated with MG132, a second proteasome inhibitor, this arrest proved more readily reversible, as expected given the inhibitory constant (Ki) values of bortezomib and MG132 (0.6 and 4 nM, respectively) (fig. S5A).

To test whether predivision cells treated with bortezomib were inhibited from undergoing DNA replication as well as cell division, as is the case for a proteasome inhibition-induced mitotic arrest in eukaryotes, we made use of a *S. acidocaldarius* mutant strain expressing thymidine kinase (STK). STK cells incorporate the thymidine analog 5-ethynyl-2'-deoxyuridine (EdU) into newly synthesized DNA, which can be visualized with click-it chemistry (see methods) (24). Using this assay, the majority of synchronized STK cells

divided and incorporated EdU into their DNA as they entered S phase [note that EdU prevents the completion of S phase in *S. acidocaldarius* (24)]. By contrast, there was no evidence of EdU incorporation, and therefore DNA synthesis, in cells treated with bortezomib before division (Fig. 1, G and H, and fig. S4, C and D). When bortezomib was added to synchronous cultures at a later stage to inhibit the proteasome in newly divided cells, however, these $G_1$ cells continued unimpeded into S phase and $G_2$ (fig. S4E). These data indicate that inhibiting proteasome activity specifically prohibits cells from dividing and also, directly or indirectly, from initiating the next round of DNA replication.

## CdvB is targeted by the proteasome during cell division

Having observed cell cycle arrest after proteasome inhibition (with bortezomib and MG132), we set out to identify proteins that are subject to proteasome-mediated degradation during cell division using tandem mass tag (TMT) labeling and quantitative mass spectrometry. Hits were identified by comparing the proteomes of bortezomib-treated synchronized cultures enriched for cells arrested before division with those of cultures 15 min after inhibitor washout, at which point most arrested cells had divided (see methods). Notably, among the large set of proteins sampled by mass spectrometry, the protein concentration that decreased the most after release from the arrest was CdvB, an ESCRT-III homolog previously identified as a component of the archaeal division machinery *(13–15, 25)* (Fig. 2A and table S6). As expected, CdvB was also identified among the top hits when the proteomes of MG132-treated predivision cultures were compared with the proteomes of DMSO-treated controls (fig. S5B and table S7). These results were confirmed by Western blotting using antibodies validated against cell extracts and purified proteins (Fig. 2B and figs. S6, A and B, and S7B; see methods). Furthermore, CdvB levels increased markedly in cells after induced expression of a Walker B dominant-negative PAN AAA+ ATPase (Saci_0656), a protein known to cap the 20S proteasome, which aids protein degradation by threading proteins into its core (8) (Fig. 2C). Notably, CdvB was the only division protein consistently enriched in these experiments (Fig. 2A and figs. S5A and S7B). CdvA (Saci_1374, an archaea-specific ESCRT-III recruitment protein), CdvC (Saci_1372, a Vps4 homolog), and CdvB1 and CdvB2 (Saci_0451 and Saci_1416, ESCRT-III homologs), were largely unaffected by proteasome inhibition. This selectivity was not due to differences in Cdv gene transcription, because all of these components of the cell division machinery are transcribed as part of the same predivision wave (13,14), which we confirmed remains active during a bortezomib-induced predivision arrest (fig. S7A). Taken together, these observations imply a role for selective proteasome-mediated degradation of CdvB at division.

We observed a similar sudden loss of CdvB protein from cells when we used flow cytometry to assess the levels of different ESCRT-III proteins in a population of unperturbed cells as they underwent division (see methods). Again, CdvB was found accumulating to high levels in predivision cells but was absent from newly divided $G_1$ cells (Fig. 2D and fig. S8C). By contrast, CdvB1 and CdvB2 were maintained at high levels throughout the division process and then partitioned between newly divided daughter cells (Fig. 2E and fig. S8, A, D, and F). In examining the dynamics of CdvB and CdvB1 levels during cell division, it also became clear that CdvB was degraded in cells with 2N DNA content, i.e., before cell division (Fig. 2, F and G, and figs. S8E and S10C). As expected, a flow cytometry analysis

of CdvB revealed increased levels in cells arrested before division by bortezomib (Fig. 2H), whereas median levels of CdvB1 and CdvB2 remained unaltered (Fig. 2, I to K, and fig. S8B). Taken together, these observations show that CdvB is selectively targeted for proteasome-mediated degradation partway through the division process.

## CdvB degradation triggers constriction of the CdvB1:CdvB2 ring

Previous studies have suggested that CdvB, an essential gene in *S. acidocaldarius*, is actively required for division (13–15, 25, 26). By contrast, our data suggest that the protein is degraded during division. To reconcile these data and understand the role of CdvB and its degradation in cell division, we used super-resolution radial fluctuations (SRRF) super-resolution microscopy to image the archaeal ESCRT-III division rings at different stages in the division process (see methods) (27, 28). This revealed three distinct categories of ESCRT-III division rings: (i) CdvB rings that lack CdvB1, (ii) rings with colocalized CdvB and CdvB1, and (iii) CdvB1 rings that lack CdvB (Fig. 3A). Conspicuously, cells harboring a CdvB1 ring, but lacking CdvB signal, were the only ones seen in a state of constriction. These data support a role for the selective proteasome-mediated degradation of CdvB from preassembled CdvB: CdvB1 rings. This is consistent with the fact that CdvB rings had a mean diameter of 1.23 μm ($n$ = 496, SD = 0.15) (Fig. 3B) and CdvB1 rings costaining for CdvB had a near-identical mean diameter of 1.24 μm ($n$ = 285, SD = 0.17), whereas CdvB1 rings that lacked CdvB tended to be variable in size and smaller (mean = 0.62 μm, $n$ = 61, SD = 0.35) (Fig. 3C).Moreover, as expected for a division ring, the diameter of the CdvB1 ring was nearly perfectly correlated with the diameter of the division neck, as measured by concanavalin A staining of the archaeal S-layer (fig. S8G). Finally, the diameters of CdvB1 and CdvB2 rings were near perfectly correlated in all images, suggesting that the two ESCRT-III homologs work together during the ring constriction stage of the division process [N = 399, correlation coefficient ($r$) = 0.98, $p = 2.2 \times 10^{-16}$] (fig. S8H). Taken together, these data suggest that constriction is triggered by the selective and rapid degradation of CdvB by the proteasome. In line with this thinking, we were unable to detect CdvB1 rings lacking CdvB (or CdvB2 rings lacking CdvB) in cells after treatment with the proteasome inhibitor bortezomib. Moreover, all of the rings in bortezomib-treated cells had a mean diameter equivalent to the uniform width of CdvB rings that span the longest axis of the cell, highlighting the role of the proteasome-mediated degradation of CdvB in triggering cell constriction (mean = 1.23 μm, $N$ = 346, SD = 0.32) (Fig. 3D).

The flow cytometry profiles of exponentially growing asynchronous populations co-stained for CdvB and CdvB1 could also be used to generate an approximate timeline of cell division events. This revealed populations of cells in three distinct phases of the division process: (i) 2N cells with peak levels of CdvB but low CdvB1, (ii) 2N cells with peak levels of both CdvB and CdvB1, and (iii) 2N cells with falling levels of CdvB that retain peak levels of CdvB1 (fig. S9A). Because the doubling time of these *S. acidocaldarius* cultures was about 2 hours and 45 min, the relative sizes of these subpopulations could be used to calculate the time spent by a typical cell in each stage of the division process. Notably, this requires taking the exponential age distribution resulting from binary division into account (fig. S9B) (29). Thus, the entire process of ESCRT-III-mediated cell division was estimated to have a duration of ~6.2 min (fig. S9, B and C) (29). The division process was further resolved on

the basis of these data to reveal the following sequence of events: (i) CdvB rings had an average lifetime of ~2.6 min, before the assembly of CdvBl, (ii) CdvB:CdvB1 rings then persisted for ~1.8 min, before CdvB was degraded by the proteasome, (iii) causing CdvB1 rings to constrict within a period of ~1.8 min. Although we observed minor variations in the percentage of cells in the other two stages of division, the percentage of cells in the contractile phase of the division process (as CdvB is being degraded) appeared highly reproducible (fig. S9C).

## Physical model of ESCRT-III-mediated cell division in Archaea

To better monitor changes in both the levels and localization of the CdvB1 ring during the final stages of the division process, we imaged fixed cells using linear structured illumination microscopy (iSIM) [see methods]. This revealed that constriction of the CdvB1 division ring was accompanied by both an increase in the intensity of the fluorescent signal at the neck and a concomitant increase in the level of the diffuse cytoplasmic signal (Fig. 4A and fig. S10A). Throughout division, the sum intensity of CdvB1 remained constant (fig. S10B). As a result, newly divided cells had high levels of diffuse CdvB1 (something we never observed imaging CdvB), in line with the flow cytometric data (Fig. 2F and fig. S8, C and D). The absence of large polymeric CdvB1:CdvB2 structures in these early $G_1$ cells implies that CdvB1 and CdvB2 do not form de novo ESCRT-III filaments without a CdvB template. In keeping with this conclusion, CdvB2 appeared diffuse when it was ectopically expressed in cells arrested in $G_2$ with acetic acid, a treatment that inhibits the expression of endogenous Cdv proteins (fig. S11, A to C). Taken together, these observations suggest that the division machinery follows a fixed sequence in which CdvB initially forms an ESCRT-III ring [in a process that likely depends on CdvA (25, 30)], which then templates the assembly of CdvB1:CdvB2 rings. This CdvB1:CdvB2 ring constricts after the sudden removal and degradation of CdvB and is then disassembled during the division process.

To test whether these findings provide a plausible physical mechanism for *S. acidocaldarius* cell division, we used these data as the basis for a coarse-grained molecular dynamics model of ESCRT-III-mediated cell division, based on a recently developed physical model of ESCRT-III-dependent membrane scission (31) (see methods). In these simulations, a modeled filament, representing the division ring, was allowed to associate with the plasma membrane of a cell modeled in three dimensions through its membrane-binding interface. To model the division process, we defined two different preferred filament conformations: a CdvB1 (CdvB+) state with low curvature (defined by a large preferred radius $R_0$) and a CdvB1 (CdvB-) state with high curvature (defined by the small target radius $R_{target}$) (Fig. 4B). In this model, the transition between the initial CdvB1 (CdvB+) state and the CdvB1 (CdvB-) state represents the rapid loss of CdvB, which was modeled by an instantaneous shortening of the bonds connecting neighboring elements in the filament. Although the constriction of the CdvB1 ESCRT-III filament was able to rapidly reduce the cell circumference in these simulations, it was not sufficient to induce division because of the steric hindrance at the neck (Fig. 4C and Movie 1, where $R_{target}/R_0 = 5\%$). This is a generic problem faced by molecular machines that cut membrane tubes from the inside. Thus, it was only when CdvB1 filaments were allowed to disassemble as they constricted, as observed in cells (Fig. 4A), that division occurred (Fig. 4D). This was modeled as a gradual loss of

individual subunits from both ends of the helix at a specified rate, such that the filament length decreases linearly in time (Movie 2, where $R_{target}/R_0 = 5\%$). In sum, these data and simulations highlight the importance of disassembling the CdvB1:CdvB2 copolymer during constriction, so that the ESCRT-III filament does not crowd the neck and prevent scission.

## Discussion

These findings demonstrate how proteasome-mediated degradation of CdvB, a component of the ESCRT-III ring, plays a key role in ordering the changes in ESCRT-III copolymer structure to drive cell division and suggest an elegant mechanism by which *S. acidocaldarius* cells divide. First, cells assemble a structural noncontractile CdvB ring at the center of the cell. This ESCRT-III filament acts as a template for the assembly of CdvB1 and CdvB2 ESCRT-III proteins, which have a smaller preferred radius of curvature. The tension stored in this CdvB1:CdvB2 polymer is then released once the CdvB template is removed and degraded by the proteasome, driving membrane constriction. During constriction, this copolymer is disassembled gradually to enable scission of the membrane bridge connecting the two nascent daughter cells.

Although we were able to demonstrate that the proteasome is able to directly degrade CdvB in vitro (fig. S12), the process is likely more complicated in vivo. This is supported by the observation that a defective PAN proteasome cap leads to an accumulation of CdvB (Fig. 2C). Moreover, previous studies have implicated the ESCRT-III-associated protein Vps4 (CdvC) in the division process (14, 32). In eukaryotes, Vps4 plays a role in the stepwise disassembly of composite ESCRT-III filaments and in membrane deformation (31,33,34). Because the role of Vps4 appears to be conserved, these data suggest that CdvC might be required to selectively extract CdvB from the composite CdvB, CdvB1:CdvB2 copolymer. This soluble pool of CdvB might then be rapidly targeted to the proteasome via PAN, and possibly other proteins, leading to its degradation before it can be reincorporated back into the ring. Although this remains speculation, under this model, the degradation of CdvB would make this change in ESCRT-III polymer structure functionally irreversible. CdvC might then also catalyze the disassembly of the CdvB1:CdvB2 polymer, which is required to vacate the division neck, thus aiding the final process of membrane scission. In line with this idea, previous studies have found that truncating the CdvC-interacting domain in CdvB, CdvB1, or CdvB2 leads to an arrest at various points during the constriction process (15), implying that CdvC plays one or more essential roles in archaeal cell division.

This study reveals that ESCRT-III-mediated cell division in *S. acidocaldarius* is regulated by the selective proteasome-mediated degradation of CdvB. It also reveals parallels between cell cycle control in archaea and eukaryotes, implying that proteasome-mediated regulation predates cyclins and cyclin-dependent kinases. Further work will be required (i) to identify all the relevant targets of the proteasome during this final cell cycle transition in Archaea, (ii) to determine whether the proteasome plays an analogous role in driving ESCRT-III-dependent cell division in eukaryotes, (iii) to determine whether the degradation of any of these proteins plays a role in resetting the archaeal cell cycle in a manner analogous the role played by cyclin degradation in eukaryotes, and (iv) to determine if there are other shared design features governing cell cycle progression across the archaeal-eukaryotic divide.




Europe PMC Funders Author Manuscripts

Europe PMC Funders Author Manuscripts

However, this study emphasizes the utility of using archaea as a simple model to explore fundamental features of eukaryotic molecular cell biology that have been conserved over 2 billion years of evolution.

## Materials and methods summary

### Cell culturing, synchronization, and drug treatments

*S. acidocaldarius* strains were grown at 75°C and pH 3.0 to 3.5 in Brock medium supplemented with NZ-amine and sucrose, with the exception of the STK and MW001 strains that were also supplemented with uracil. Synchronization was achieved with acetic acid treatment and proteasome inhibition by supplementing bortezomib or MG132.

### Biochemistry and mass spectrometry

Biochemical analyses were carried out on extracted protein by Western blotting and mass spectrometry and on RNA by quantitative polymerase chain reaction (qPCR). In vitro assays of proteasome activity were studied in the context of active and inactive proteasome assemblies supplemented with a 3xUrm1-GFP reporter. Proteins of interest were expressed in *Escherichia coli*. The antibody specificities for CdvB, CdvB1, and CdvB2 were tested by enzyme-linked immunosorbent assay (ELISA) and whole Western blots.

### S. acidocaldarius genetics

Two overexpression strains were generated: (i) a dominant negative PAN-WalkerB-HA (HA, hemagglutinin) and (ii) a wild-type CdvB2. Both proteins were subject to arabinose induction and maintained on a plasmid complementing the strains' uracil auxotrophy.

### Microscopy and flow cytometry

All microscopy and flow cytometry studies were done on ethanol-fixed cells, staining for DNA and the S-layer and with antibodies CD against ESCRT-III homologs. For super-resolution, SRRF and linear iSIM were used.

### Crystallography

The inactive proteasome subunits were over-expressed in and purified from *E. coli*. Subsequently, crystals were grown in CZ buffer (see methods), and a 3.7-Å dataset was collected from a single crystal at SOLEIL, France.

### Molecular dynamics simulations

A fluid spherical membrane consisting of 48,000 particles was modeled together with a chiral ESCRT-III filament modeled with three-beaded subunits (31). Simulations for the constriction and disassembly of the ESCRT-III filament were run with the LAMMPS molecular dynamics package.

## Supplementary Material

Refer to Web version on PubMed Central for supplementary material.

## Acknowledgments

We thank the MRC LMCB at UCL for their support; the flow cytometry STP at the Francis Crick Institute for assistance, with special thanks to S. Purewal and D. Davis; C. Bertoli for mentorship and advice; J. M. Garcia-Arcos for help early on in this project; the entire Baum lab for their input throughout the project; the Albers lab for advice and reagents, with special thanks to M. Van Wolferen and S. Albers; the members of the Wellcome consortium for archaeal cytoskeleton studies for advice and comments; and J. Lowe, S. Oliferenko, M. Balasubramanian, and D. Gerlich for discussions and advice on the manuscript. N.P.R. and S.B. would like to thank N. Rzechorzek, A. Simon, and S. Anjum for discussion and advice.

### Funding

The Baum, Henriques, and de Bruin labs received support from the MRC (MC_CF12266). G.T.R. was supported by MRC (1621658). F.H. was supported by Vetenskapsradet (621-2013-4685) and A.A.P. by the HFSP (LT001027/2019 fellowship).A collaborative grant from the Wellcome Trust supported A.A.P., D.P.S., G.D., S.C., and the Baum, Lindas, and Henriques labs (203276/Z/16/Z). D.R.M. was supported by a BBSRC grant awarded to B.B. (BB/K009001/1). L.M. and R.A.M.d.B. were supported by Cancer Research UK (C33246/A20147). P.F., C.D., and A.P.S. were supported by the Francis Crick Institute, which receives its core funding from Cancer Research UK (FC001999), the UK Medical Research Council (FC001999), and the Wellcome Trust (FC001999). L.H.-K. was supported by the Biotechnology and Biological Sciences Research Council (BB/M009513/1). A.Š. and A.E.H. were supported by the European Research Council (802960) and the Engineering and Physical Sciences Research Council (EP/R011818/1). N.P.R. was supported by the Isaac Newton Trust Research Grant (Trinity College and Department of Biochemistry, Cambridge) and start-up funds from the Division of Biomedical and Life Sciences (Lancaster University) and received a BBSRC Doctoral Training Grant (RG53842) for S.B.

## Data and materials availability

All data are available in the manuscript or the supplementary materials. The crystal structure of the *S. acidocaldarius* 20*S* proteasome is available at PDB, with the ID 6Z46. All materials are available from B.B. or N.P.R. on request.

## References and Notes

1. Bernander R. The cell cycle of Sulfolobus. Mol Microbiol. 2007; 66:557–562. DOI: 10.1111/j.1365-2958.2007.05917.x [PubMed: 17877709]
2. Ausiannikava D, Allers T. Diversity of DNA replication in the Archaea. Genes. 2017; 8:56.doi: 10.3390/genes8020056
3. Lang S, Huang L. The Sulfolobus solfataricus GINS complex stimulates DNA binding and processive DNA unwinding by minichromosome maintenance helicase. J Bacteriol. 2015; 197:3409–3420. DOI: 10.1128/JB.00496-15 [PubMed: 26283767]
4. Caspi Y, Dekker C. Dividing the archaeal way: The ancient Cdv cell-division machinery. Front Microbiol. 2018; 9:174.doi: 10.3389/fmicb.2018.00174 [PubMed: 29551994]
5. Groll M, Brandstetter H, Bartunik H, Bourenkow G, Huber R. Investigations on the maturation and regulation of archaebacterial proteasomes. J Mol Biol. 2003; 327:75–83. DOI: 10.1016/S0022-2836(03)00080-9 [PubMed: 12614609]
6. Löwe J, et al. Crystal structure of the 20S proteasome from the archaeon acidophilum T. acidophilum at 3.4 Å resolution. Science. 1995; 268:533–539. DOI: 10.1126/science.7725097 [PubMed: 7725097]
7. Zhang F, et al. Structural insights into the regulatory particle of the proteasome from Methanocaldococcus jannaschii. Mol Cell. 2009; 34:473–484. DOI: 10.1016/j.molcel.2009.04.021 [PubMed: 19481527]
8. Maupin-Furlow J. Proteasomes and protein conjugation across domains of life. Nat Rev Microbiol. 2011; 10:100–111. DOI: 10.1038/nrmicro2696 [PubMed: 22183254]
9. Giménez-Abián JF, Diaz-Martínez LA, Wirth KG, De la Torre C, Clarke DJ. Proteasome activity is required for centromere separation independently of securin degradation in human cells. Cell Cycle. 2005; 4:1558–1560. DOI: 10.4161/cc.4.11.2145 [PubMed: 16205121]

10. López-Aviles S, Kapuy O, Novák B, Uhlmann F. Irreversibility of mitotic exit is the consequence of systems-level feedback. Nature. 2009; 459:592–595. DOI: 10.1038/nature07984 [PubMed: 19387440]
11. Glotzer M, Murray AW, Kirschner MW. Cyclin is degraded by the ubiquitin pathway. Nature. 1991; 349:132–138. DOI: 10.1038/349132a0 [PubMed: 1846030]
12. Wickliffe K, Williamson A, Jin L, Rape M. The multiple layers of ubiquitin-dependent cell cycle control. Chem Rev. 2009; 109:1537–1548. DOI: 10.1021/cr800414e [PubMed: 19146381]
13. Lindås A-C, Karlsson EA, Lindgren MT, Ettema TJG, Bernander R. A unique cell division machinery in the Archaea. Proc Natl Acad Sci U.S.A. 2008; 105:18942–18946. DOI: 10.1073/pnas.0809467105 [PubMed: 18987308]
14. Samson RY, Obita T, Freund SM, Williams RL, Bell SD. A role for the ESCRT system in cell division in Archaea. Science. 2008; 322:1710–1713. DOI: 10.1126/science.1165322 [PubMed: 19008417]
15. Liu J, et al. Functional assignment of multiple ESCRT-III homologs in cell division and budding in Sulfolobus islandicus. Mol Microbiol. 2017; 105:540–553. DOI: 10.1111/mmi.13716 [PubMed: 28557139]
16. Anjum RS, et al. Involvement of a eukaryotic-like ubiquitin-related modifier in the proteasome pathway of the archaeon Sulfolobus acidocaldarius. Nat Commun. 2015; 6:8163.doi: 10.1038/ncomms9163 [PubMed: 26348592]
17. Šali A, Blundell TL. Comparative protein modelling by satisfaction of spatial restraints. J Mol Biol. 1993; 234:779–815. DOI: 10.1006/jmbi.1993.1626 [PubMed: 8254673]
18. Adams J, et al. Proteasome inhibitors: A novel class of potent and effective antitumor agents. Cancer Res. 1999; 59:2615–2622. [PubMed: 10363983]
19. Chen D, Frezza M, Schmitt S, Kanwar J, Dou QP. Bortezomib as the first proteasome inhibitor anticancer drug: Current status and future perspectives. Curr Cancer Drug Targets. 2011; 11:239–253. DOI: 10.2174/156800911794519752 [PubMed: 21247388]
20. Fu X, et al. Ubiquitin-like proteasome system represents a eukaryotic-like pathway for targeted proteolysis in Archaea. mBio. 2016; 7:e00379–e16. DOI: 10.1128/mBio.00379-16 [PubMed: 27190215]
21. Hepowit NL, Maupin-Furlow JA. Rhodanese-like domain protein UbaC and its role in ubiquitin-like protein modification and sulfur mobilization in Archaea. J Bacteriol. 2019; 201:e00254–19. DOI: 10.1128/JB.00254-19 [PubMed: 31085691]
22. Oerlemans R, et al. Molecular basis of bortezomib resistance: Proteasome subunit p5 (PSMB5) gene mutation and overexpression of PSMB5 protein. Blood. 2008; 112:2489–2499. DOI: 10.1182/blood-2007-08-104950 [PubMed: 18565852]
23. Lundgren M, Andersson A, Chen L, Nilsson P, Bernander R. Three replication origins in Sulfolobus species: Synchronous initiation of chromosome replication and asynchronous termination. Proc Natl Acad Sci USA. 2004; 101:7046–7051. DOI: 10.1073/pnas.0400656101 [PubMed: 15107501]
24. Gristwood T, Duggin IG, Wagner M, Albers SV, Bell SD. The sub-cellular localization of Sulfolobus DNA replication. Nucleic Acids Res. 2012; 40:5487–5496. DOI: 10.1093/nar/gks217 [PubMed: 22402489]
25. Samson RY, et al. Molecular and structural basis of ESCRT-III recruitment to membranes during archaeal cell division. Mol Cell. 2011; 41:186–196. DOI: 10.1016/j.molcel.2010.12.018 [PubMed: 21255729]
26. Yang N, Driessen AJM. Deletion of cdvB paralogous genes of Sulfolobus acidocaldarius impairs cell division. Extremophiles. 2014; 18:331–339. DOI: 10.1007/s00792-013-0618-5 [PubMed: 24399085]
27. Gustafsson N, et al. Fast live-cell conventional fluorophore nanoscopy with ImageJ through super-resolution radial fluctuations. Nat Commun. 2016; 7:12471.doi: 10.1038/ncomms12471 [PubMed: 27514992]
28. Laine RF, et al. NanoJ: a high-performance open-source super-resolution microscopy toolbox. bioRxiv. 2018 Oct 6.doi: 10.1101/432674

29. Wold S, Skarstad K, Steen HB, Stokke T, Boye E. The initiation mass for DNA replication in Escherichia coli K-12 is dependent on growth rate. EMBO J. 1994; 13:2097–2102. DOI: 10.1002/j.1460-2075.1994.tb06485.x [PubMed: 8187762]

30. Dobro MJ, et al. Electron cryotomography of ESCRT assemblies and dividing Sulfolobus cells suggests that spiraling filaments are involved in membrane scission. Mol Biol Cell. 2013; 24:2319–2327. DOI: 10.1091/mbc.e12-11-0785 [PubMed: 23761076]

31. Harker-Kirschneck L, Baum B, Saric AE. Changes in ESCRT-III filament geometry drive membrane remodelling and fission in silico. BMC Biol. 2019; 17:82.doi: 10.1186/s12915-019-0700-2 [PubMed: 31640700]

32. Mierzwa BE, et al. Dynamic subunit turnover in ESCRT-III assemblies is regulated by Vps4 to mediate membrane remodelling during cytokinesis. Nat Cell Biol. 2017; 19:787–798. DOI: 10.1038/ncb3559 [PubMed: 28604678]

33. Pfitzner A-K, Mercier V, Roux A. Vps4 triggers sequential subunit exchange in ESCRT-III polymers that drives membrane constriction and fission. bioRxiv. 2019 Jul 29.doi: 10.1101/718080

34. Caillat C, Maity S, Miguet N, Roos WH, Weissenhorn W. The role of VPS4 in ESCRT-III polymer remodeling. Biochem Soc Trans. 2019; 47:441–448. DOI: 10.1042/BST20180026 [PubMed: 30783012]

Europe PMC Funders Author Manuscripts

Europe PMC Funders Author Manuscripts

**Introduction**

Eukaryotes likely arose from a symbiotic partnership between an archaeal host and an alpha-proteobacterium, giving rise to the cell body and the mitochondria, respectively. Because of this, a number of proteins controlling key events in the eukaryotic cell division cycle have their origins in archaea. These include ESCRT-III proteins, which catalyze the final step of cytokinesis in many eukaryotes and in the archaeon *Sulfolobus acidocaldarius*. However, to date, no archaeon has been found that harbors homologs of cell cycle regulators, like cyclin-dependent kinases and cyclins, which order events in the cell cycle across all eukaryotes. Thus, it remains uncertain how key events in the archaeal cell cycle, including division, are regulated.

**Rationale**

An exception to this is the 20S proteasome, which is conserved between archaea and eukaryotes and which regulates the eukaryotic cell cycle through the degradation of cyclins. To explore the function of the 20*S* proteasome in the archaeon *S. acidocaldarius*, we determined its structure by crystallography and carried out in vitro biochemical analyses of its activity with and without inhibition. The impact of proteasome inhibition on cell division and cell cycle progression was examined in vivo by flow cytometry and super-resolution microscopy. Following up with mass spectrometry, we identified proteins degraded by the proteasome during division. Finally, we used molecular dynamics simulations to model the mechanics of this process.

**Results**

Here, we present a structure of the 20S proteasome of *S. acidocaldarius* to a resolution of 3.7 Å, which we used to model its sensitivity to the eukaryotic inhibitor bortezomib. When this inhibitor was added to synchronous cultures, it was found to arrest cells middivision, with a stable ESCRT-III division ring positioned at the cell center between the two separated and prereplicative nucleoids. Proteomics was then used to identify a single archaeal ESCRT-III homolog, CdvB, as a key target of the proteasome that must be degraded to enable division to proceed.

Examining the localization patterns of CdvB and two other archaeal ESCRT-III homologs, CdvBl and CdvB2, by flow cytometry and superresolution microscopy revealed the sequence of events that leads to division. First, a CdvB ring is assembled. This CdvB ring then templates the assembly of the contractile ESCRT-III homologs, CdvBl and CdvB2, to form a composite division ring. Cell division is then triggered by proteasome-mediated degradation of CdvB, which allows the CdvB1:CdvB2 copolymer to constrict, pulling the membrane with it. During constriction, the CdvB1:CdvB2 copolymer is disassembled, thus vacating the membrane neck to drive abscission, yielding two daughter cells with diffuse CdvBl and CdvB2.

**Conclusion**

This study reveals a role for the proteasome in driving structural changes in a composite ESCRT-III copolymer, enabling the stepwise assembly, disassembly, and contraction of an ESCRT-III-based division ring. Although it is not yet clear how proteasomal inhibition

prevents *S. acidocaldarius* cells from resetting the cell cycle to initiate the next S phase, these data strengthen the case for the eukaryotic cell cycle regulation having its origins in archaea.



Europe PMC Funders Author Manuscripts

Europe PMC Funders Author Manuscripts

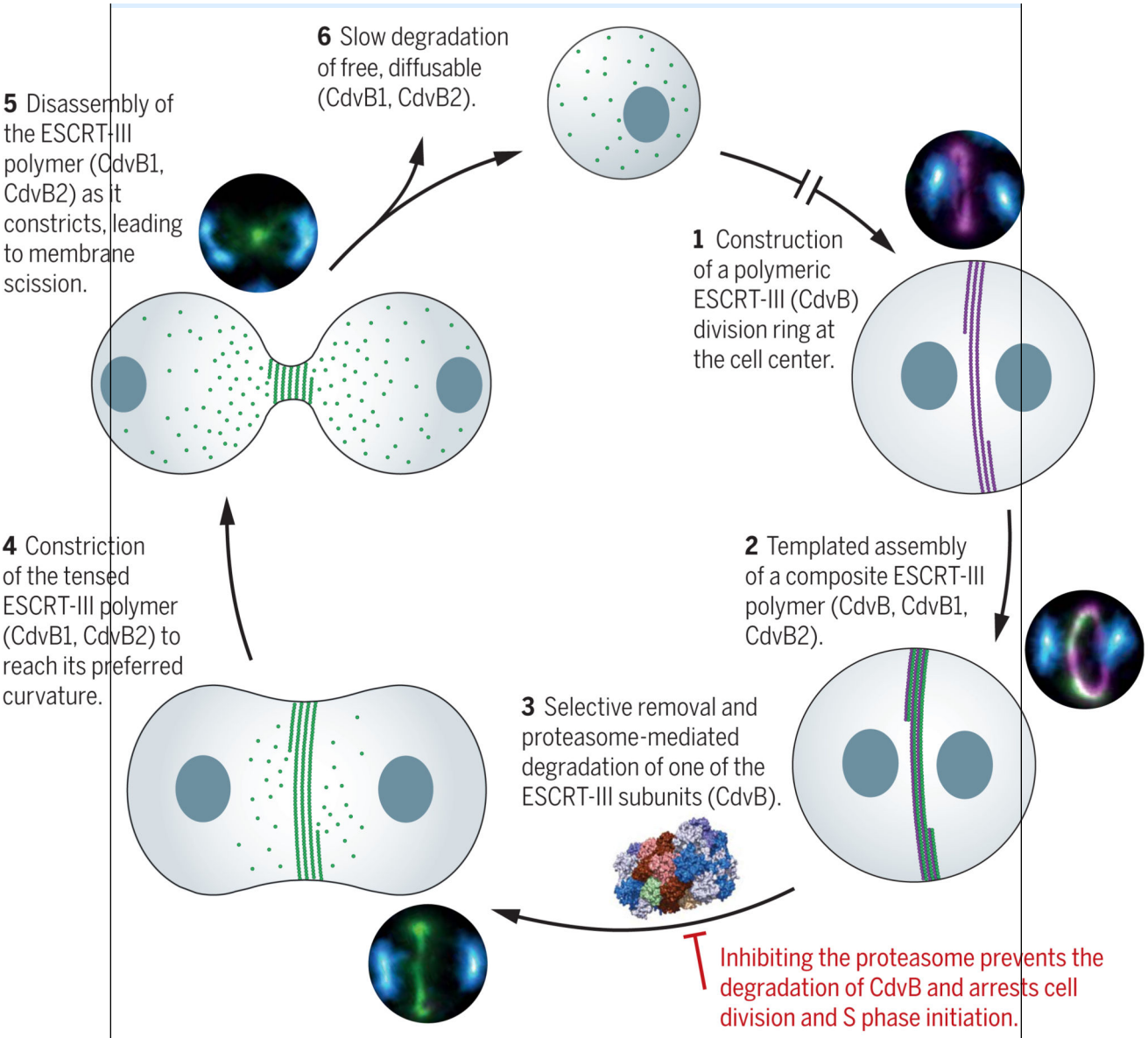


**Model of ESCRT-III-mediated cell division in the archaeon *S. acidocaldarius***

The model shows the sequential stages of the division process in *S. acidocaldarius* (labeled 1 to 6), together with the corresponding stage-specific images. DNA is in blue, CdvB in purple, and CdvB1 and CdvB2 in green. The broken arrow represents an extended period where cells progress through $G_1$, S, and $G_2$. Note that Vps4 (not shown) is likely required for ESCRT-III polymer disassembly.

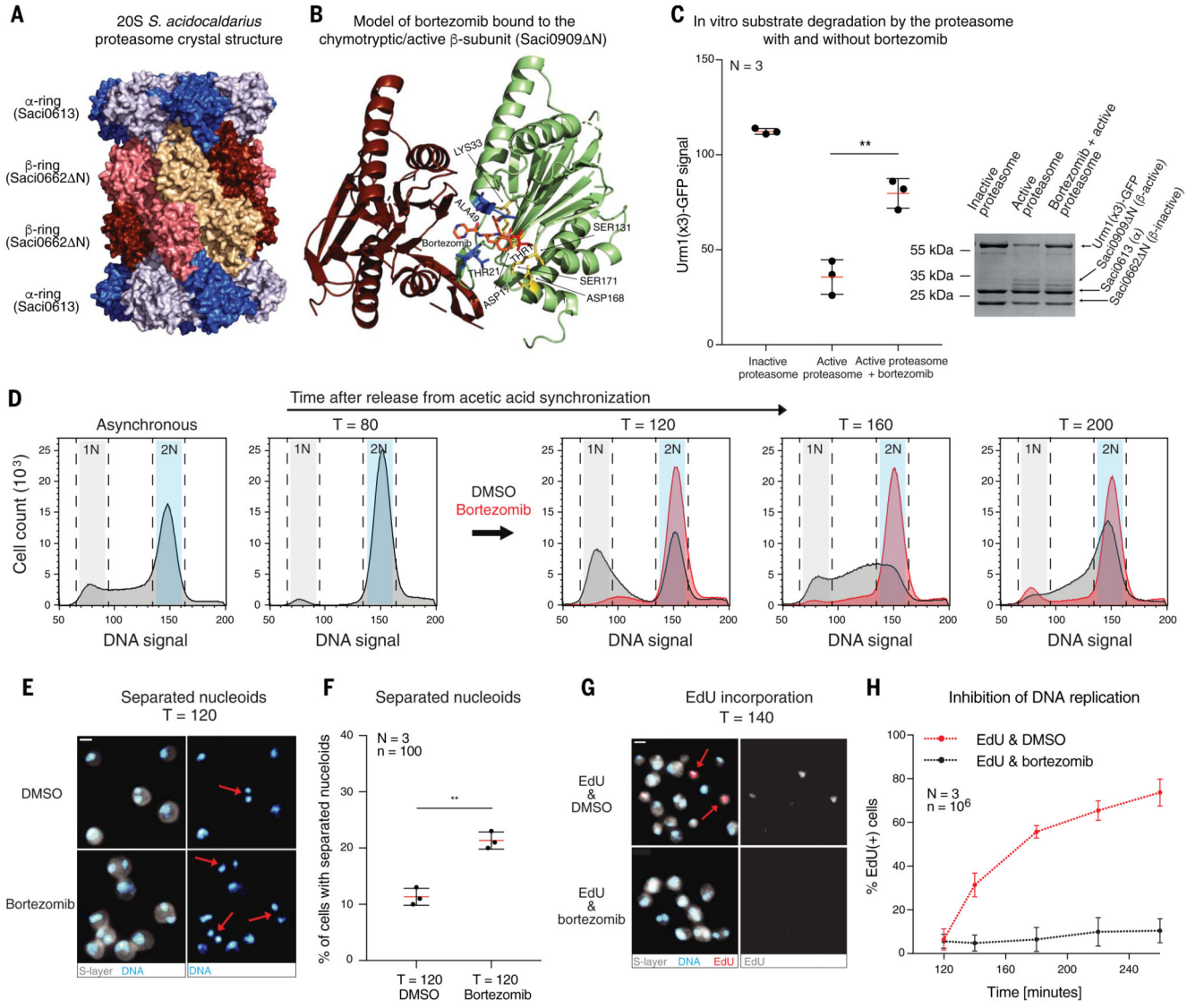


**Fig. 1. *S.acidocaldarius* cell division is arrested after inhibition of the proteasome.**

(**A**) Side view of the *S. acidocaldarius* 28-subunit Saci_0613/Saci_0662ΔN 20S proteasome assembly. Saci_0613 α subunits are indicated by blue and purple hues; Saci_0662ΔN β subunits are indicated by red, pink, and beige hues. (**B**) Modeled binding of the reversible inhibitor bortezomib to the active β subunit (Saci_ΔN) chymotryptic site in the *S. acidocaldarius* 20S proteasome using the CovDock software. The catalytic threonine ($Thr^1$) is shown as a red stick covalently bound to the boronic acid group of the bortezomib molecule. The $Asp^{17}$, $Lys^{33}$, $Ser^{129}$, $Asp^{166}$, and $Thr^{169}$ involved in catalysis are shown as yellow sticks. The two loops (blue) harboring the conserved residues $Ala^{20}$, $Ser^{21}$, and $Gly^{47}$ to $Val^{49}$ mediate binding of the inhibitor. (**C**) Quantified degradation assay of GFP control or Urm1(x3)-GFP substrate by the Saci_0613/Saci_0662ΔN/Saci_0909ΔN 20S proteasome. Error bars represent means ± SD from $N = 3$. Data were analyzed using Welch's $t$ test; $^{**}p = 0.0034$. (**D**) Flow cytometry histograms showing 1N and 2N DNA signals in cells in an asynchronous and a synchronized population treated with bortezomib or DMSO 80 min after

release (before division). $N = 3$, and $n = 10^5$. Representative histograms are shown. T, time after release. (**E**) Wide-field microscopy images of synchronized cells treated with DMSO or bortezomib for 40 min, 80 min after release from acetic acid. Fixed cells were stained with Hoechst to visualize DNA and concanavalin A to visualize the S-layer. Red arrows indicate cells with separated nucleoids. Representative images are shown. Scale bar, 1 μm. (**F**) Quantification of the percentage of cells in synchronized populations harboring separated nucleoids after treatment with DMSO or bortezomib. Error bars represent means ± SD from $N = 3$ and $n = 100$. Data were analyzed using a ratio paired $t$ test; $^{**}p = 0.0069$. (**G**) Wide-field microscopy images of synchronized STK cells treated for 40 min with DMSO or bortezomib, 100 min after release from acetic acid. Cells were stained with Hoechst to visualize DNA and concanavalin A to visualize the S-layer, and “click” chemistry was used to visualize EdU. Red arrows indicate the cells with EdU incorporated into newly synthesized DNA. Scale bar, 1 μm. (**H**) Quantification of the percentage of synchronized cells with incorporated EdU after DMSO or bortezomib treatment. Error bars represent means ± SD from $N = 3$ and $n = 10^6$.

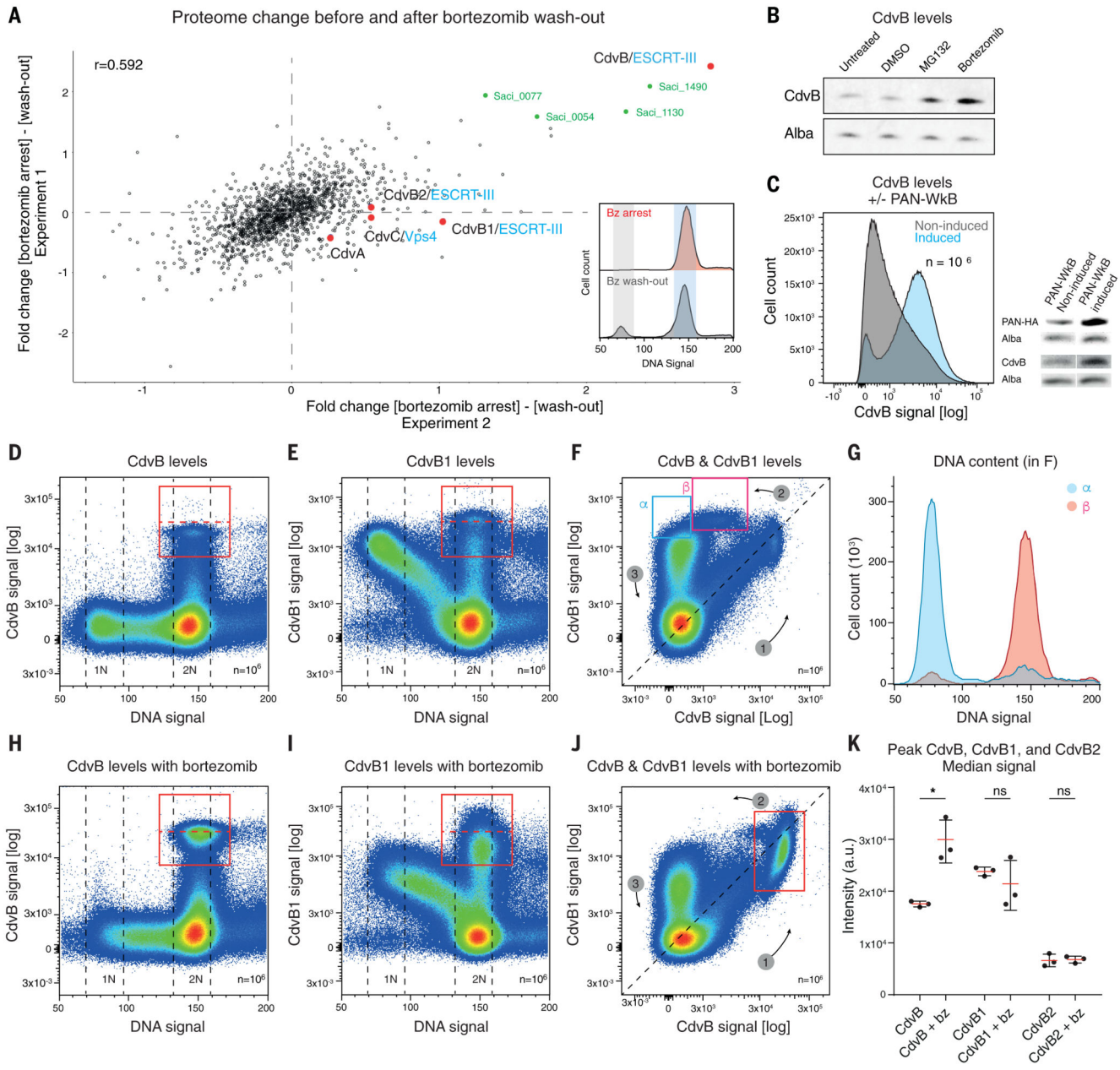


**Fig. 2. CdvB is targeted by the *S. acidocaldarius* proteasome during cell division.**

(**A**) Mass spectrometry scatterplot correlating two independent replicates of proteome changes in predivision synchronized cells treated with bortezomib for 40 min versus the population 15 min after bortezomib had been washed out (after division). The top five hits are in green (apart from CdvB). See table S6 for the complete data. The inset shows two representative histograms of the bortezomib-treated and wash-out samples. (**B**) Western blots of CdvB and Alba (loading control) for synchronized cells which, 80 min after release from acetic acid, were left untreated or treated for 40 min with DMSO, MG132, or bortezomib. (**C**) (Left) Flow cytometry histogram comparing the CdvB signal under noninduced and induced conditions for a PAN-WkB-HA dominant negative overexpression




Europe PMC Funders Author Manuscripts

strain and (right) Western blots showing the change in PAN-WkB-HA and CdvB protein levels. (**D** and **E**) Flow cytometry scatterplots of DNA versus CdvB (D) and CdvB1 (E) protein signals of cells in an asynchronous culture. The red boxes highlight the “mitotic” cells with high CdvB and CdvB1 signals in (D) and (E), respectively. Each blue spot represents a single cell, with the density gradient going from blue to red. Representative plots are shown; $N = 3$, and $n = 10^6$. (**F**) Flow cytometry scatterplot of the CdvB versus CdvB1 signal of an asynchronous culture showing the alternating accumulation and loss of the proteins. $N = 3$, and $n = 10^6$. (**G**) Flow cytometry histogram of the DNA distribution of cells in the boxes shown in (F), showing the shift from 2N to 1N taking place only after complete CdvB degradation.(**H** and **I**) Flow cytometry scatterplots of DNA versus CdvB and CdvB1 signals for an asynchronous culture treated with bortezomib. Representative plots are shown; $N = 3$, and $n = 10^6$. (**J**) Flow cytometry scatterplot of CdvB versus CdvB1 levels in an asynchronous culture treated with bortezomib showing an accumulation of cells expressing CdvB and CdvB1 and the selective increase in CdvB levels. Representative plot is shown; $N = 3$, and $n = 10^6$. (**K**) Quantification of median CdvB, CdvB1, and CdvB2 signals in the mitotic populations. Data were analyzed using a ratio paired two-tailed *t* test for CdvB with and without bortezomib (bz); $*p = 0.0245$. Error bars represent means ± SD from $N = 3$. ns, not significant; a.u., arbitrary units.

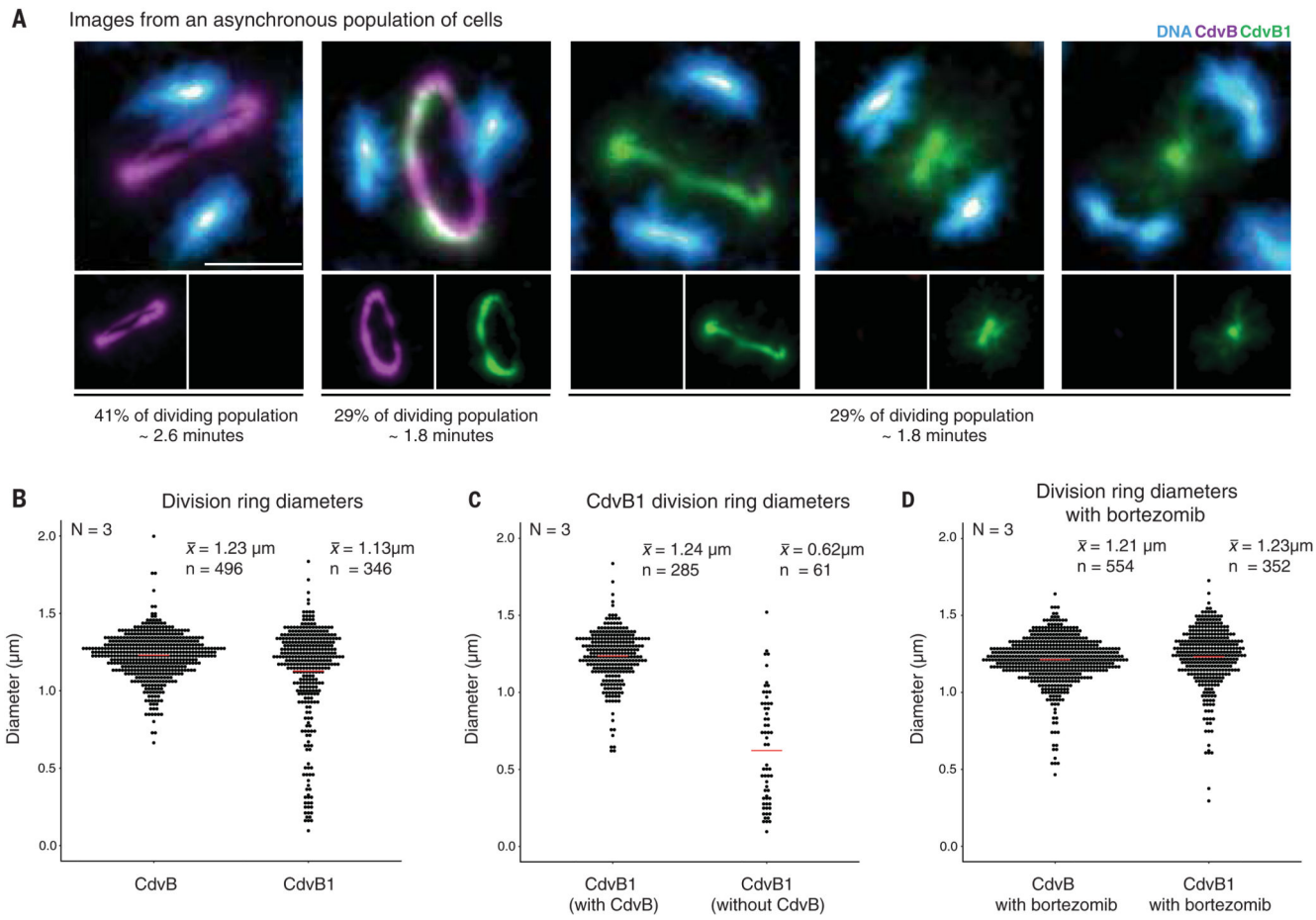


**Fig. 3. Targeted degradation of CdvB triggers constriction of CdvB1.**

(**A**) Representative SRRF super-resolution images of ring structures observed in exponentially growing asynchronous cell cultures. Cells were stained for DNA with Hoechst (blue), CdvB (purple), and CdvB1 (green); the images below the composites represent the CdvB (left) and CdvB1 (right) channels. Percentages refer to the total ring-bearing population. Minutes of the total cell cycle are adjusted for the exponential (binary fission) age distribution. Scale bar, 0.5 µm. (**B**) Quantification of CdvB and CdvB1 ring diameters in an asynchronous culture. $\overline{X}$, mean ring diameters. (**C**) Quantification of ring diameters of CdvB and CdvB1 in the presence and absence of a CdvB ring, showing how the removal of CdvB leads to constriction of CdvB1. (**D**) Quantification of ring diameters of CdvB and CdvB1 in the presence of the proteasomal inhibitor bortezomib. The data in (B) to (D) all stem from more than six fields of view and three biological replicates. Red bars represent the mean values.




Europe PMC Funders Author Manuscripts

Europe PMC Funders Author Manuscripts

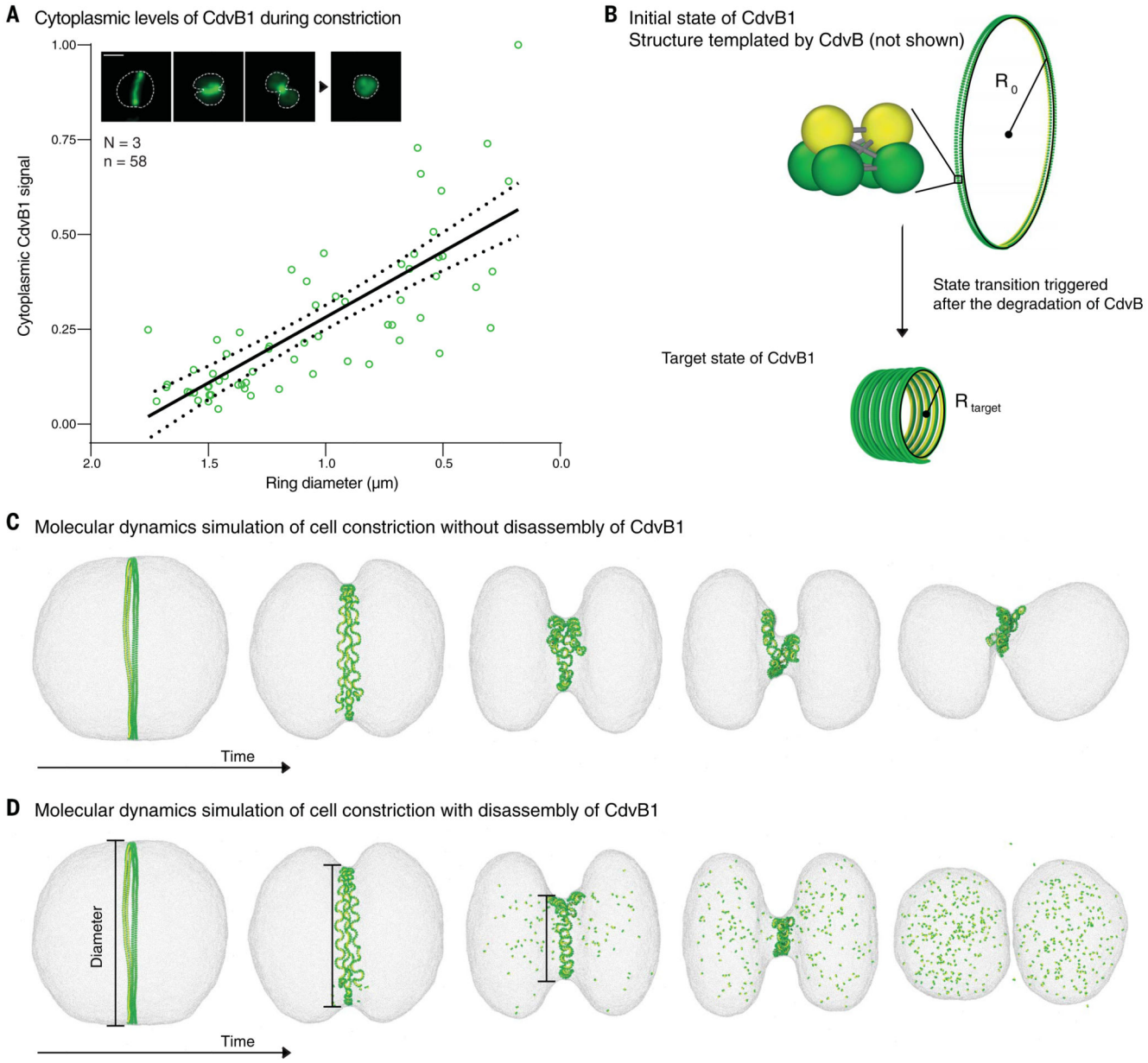


**Fig. 4. Physical model of ESCRT-III-mediated cell division in Archaea.**

(**A**) Quantification of cytoplasmic CdvB1 signal plotted against the CdvB1 ring diameter from a linear iSIM microscopy dataset, with linear regression with 95% confidence interval shown in black. The inset shows representative linear iSIM microscopy images of CdvB1 at various stages of constriction and a cell in $G_1$ after division. The outline of each cell is highlighted with a white dashed line. Scale bar, 1 μm. (**B**) The molecular dynamics simulation of the ESCRT-III filament is built with three-beaded subunits, which are connected by harmonic springs to form a helix. Only the green beads are attracted by the modeled cell membrane. The helix undergoes a geometrical change from a state with low curvature $1/R_0$, corresponding to CdvB1 with CdvB, to a state with high curvature $1/R_{\text{target}}$, corresponding to CdvB1 without CdvB. This change occurs after the proteasomal

degradation of CdvB. (**C**) Simulation snapshots as a function of time showing that cell division is not achieved by constriction of the ESCRT-III filament alone; see Movie 1. (**D**) Simulation snapshots showing that disassembly of the ESCRT-III filament is necessary for cell division; see Movie 2.



Europe PMC Funders Author Manuscripts